Available online at www.sciencedirect.com
ScienceDirect
Ceramics International 36 (2010) 589–594
CERAMICS INTERNATIONAL
www.elsevier.com/locate/ceramint

Phase transformation and morphological evolution of electrospun zirconia nanofibers during thermal annealing

Luping Li, Peigen Zhang, Jiandong Liang, S.M. Guo *

Department of Mechanical Engineering, Louisiana State University, Baton Rouge, LA 70803, USA

Received 22 July 2009; received in revised form 13 August 2009; accepted 21 September 2009
Available online 29 October 2009

Abstract

Pure zirconia nanofibers were fabricated by electrospinning zirconia-polymer precursor and subsequent annealing. Fiber properties such as polymer decomposition, crystallization formation, phase transformation, surface morphologies, etc., were investigated by various techniques, including thermogravimetric analysis (TGA) and differential thermal analysis (DTA), high temperature differential scanning calorimeter (HTDSC), powder X-ray diffractometer (XRD), field emission scanning electron microscopy (FESEM), etc. It was found that the crystallization of as-spun fibers started at 450 °C and the initial crystallized zirconia phase was tetragonal (t), which began transforming to monoclinic (m) phase at 650 °C as evidenced by XRD; HTDSC showed at different thermal circles, the m-to-t transformation temperatures remained virtually unchanged while the reverse t-to-m temperatures systematically shifted from 924.9 to 978.6 °C as the progress of thermal circles; FESEM examinations revealed that fibers calcined to 1000 °C went through thermal grooving due to surface diffusion during heat treatment; fibers heated to 1370 °C formed the so-called ''bamboo wires'', where volume diffusion was the dominant driving force.

Keywords: A. Electrospinning; B. Zirconia nanofibers; C. Phase transition; Grain growth

1. Introduction

In recent years, there has been increased interest in fabrication and investigation of one-dimensional nanostructured materials, or more specifically, nanofibers due to both scientific needs and practical demands. Those nanofibers often find their applications in microelectronics, catalysts, hydrogen-storage systems, micro-fluidics, sensors, and medical and pharmaceutical fields. Electrospinning represents a simple and promising method for fabricating nanofibers [1]. In a typical electrospinning process, a polymer-containing precursor undergoes turbulent whipping and branching when extracted by a sufficiently high electric field, leading to the formation of a nonwoven mat of nanofibers. Electrospinning is reportedly the only technique that realized the fabrication of continuous fibers in nanoscale [2].

Zirconia has been extensively investigated because of its technical importance and broad practical applications [3,4], such as thermal barrier coatings [5], electrolytes and anodes in solid oxide fuel cells [6,7], gas sensors [8], gate dielectrics [9], catalysts [10], ceramic biomaterial [11], glass ceramics [12] and so on. Its unique properties such as high toughness and chemical stability [13], good refractory properties, good ionic conductivity at high temperatures are largely based on the crystal structures of zirconia [14]. It is well established that under atmospheric pressure pure zirconia takes on three polymorphic phases: monoclinic (m), tetragonal (t), and cubic (c) [15]. M-phase is the common room-temperature stable form; m-to-t transformation takes place reversibly at ~1170 °C, and then to c-phase at ~2350 °C [16]. T-to-m transition in zirconia is one of the effective ways to improve its mechanical properties [17].

Although powder- and solid-form of zirconia has been widely investigated in terms of grain sizes and crystalline phases, phase transformation energetics, particle morphologies, etc. [4], these properties were rarely reported on nanofibrous zirconia materials. In the present work, polymer-containing zirconia nanofibers were prepared on a large scale and their thermal behaviors, phase transitions and surface characteristics, etc., were examined and reported.

* Corresponding author. Tel.: +1 225 578 7619; fax: +1 225 578 5924.
E-mail address: sguo2@lsu.edu (S.M. Guo).

0272-8842/$36.00
doi:10.1016/j.ceramint.2009.09.030

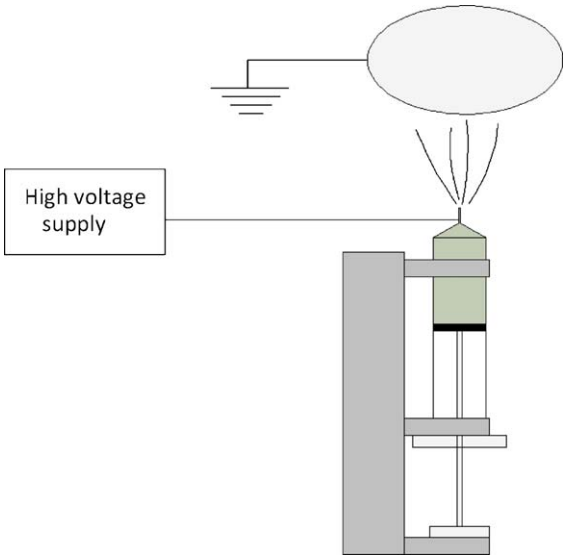

Fig. 1. Schematic of the electrospinning rig setup employed in this study.

2. Experimental

2.1. Electrospinning rig setup

A novel "spinning upwards" apparatus, as sketched in Fig. 1, was used in this study as opposed to the conventional setup of spinning sideways or downwards as described by other authors [18–21]. When compared with spinning sideways, this configuration aligned the precursor's electrical force with gravity, which was found to yield more uniform fibers; it also avoided contamination and destruction of spun-membrane by possible droplets dripping down from needle tip because of excess precursor supply in spinning downwards setup.

2.2. Zirconia nanofiber preparation

Zirconia-polymer nanofibers were fabricated by using the above-mentioned electrospinning apparatus. The precursor preparation and process parameters described below reflected the optimal combinations that led to the production of uniform and continuous fibers. 17 wt% of Polyvinylpyrrolidone (PVP) solution was first prepared by dissolving PVP (Sigma–Aldrich, USA, molecular weight 1.3 million) in ethanol to form a clear and thick mixture. Zirconia dispersion (Nyacol Nano Technologies, USA, wt% = 20%, particle size 5–10 nm) was then added to the prepared PVP solution in a weight ratio of 4.9:1. The mixed precursor was ultrasonicated for 3 min and was then stirred for 1 h on a magnetic stirrer before loading into the electrospinning rig. The typical working voltage, feeding rate, and tip-to-plate distance during electrospinning were 6.2 kV, 2 ml/h, and 8 cm, respectively.

2.3. Fiber characterizations

The as-spun nanofibers were collected from the grounded aluminum plate and cut and rolled into different shapes for various inspections. Fiber surface characteristics were examined by using a field emission scanning electron microscopy (FESEM) (Model Quanta 3D FEG, FEI Company, USA); powder X-ray diffraction (XRD) measurements were performed on an X-ray diffractometer (MiniFlex XRD, Rigaku Corporation, Japan) with Ni-filtered Cu Kα radiation (λ = 1.54178 Å). For all samples, XRD spectra were obtained by scanning over 2θ angles of 20–80° at scanning speed of 2°/min and step width of 0.02°; fibers' thermal behaviors were inspected by a thermogravimetric analyzer (TGA) (Model Q50, TA Instruments, USA) in the temperature range of 25–1000 °C; high temperature differential scanning calorimeter (HTDSC) (Model DSC 404 F1 Pegasus, NETZSCH Group, Germany) was employed to examine fibers' thermodynamic behaviors. Platinum pans were used for all HTDSC testing instead of alumina ones because the former were found to give more remarkable peak events, which was attributed to platinum's better thermal conductivity and thus being more responsive to changes of heat flow in the process of the measurements. Before each sample measurement, a baseline run was conducted and recorded using two empty pans under the same experimental conditions as would be used later for sample testing. In a typical HTDSC testing, 15 mg of as-spun zirconia nanofibers was loaded. No isothermal processes were used during HTDSC calcinations, i.e., all samples were heated to the end temperatures and cooled down immediately. Both TGA and HTDSC analyses were repeated several times to ensure good reproducibility.

3. Results and discussion

3.1. TGA and first-run HTDSC analysis

Typical TGA and DTA analysis (top) and the first-run HTDSC curve (bottom) are shown in Fig. 2. For both TGA and HTDSC testing, heating rate was 10 °C/min and air flow rate

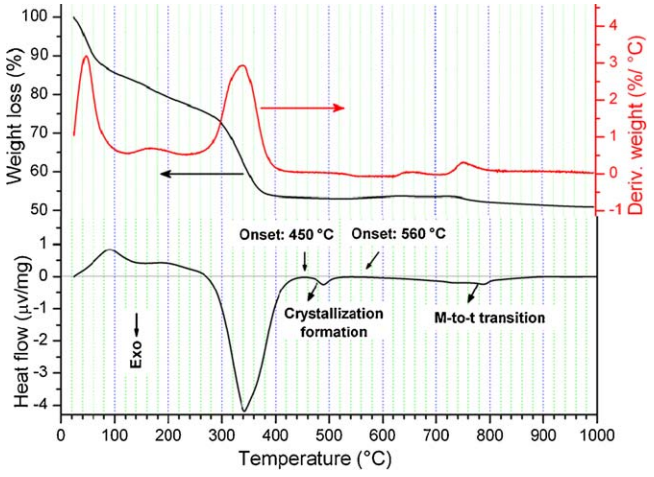

Fig. 2. TGA combined with DTA curves (top) and first-run HTDSC graph (bottom) of as-spun zirconia-polymer nanofibers. The two strong peaks on DTA curve are attributed to residual moisture evaporation and PVP polymer decomposition, respectively; the exothermic peak starting at 450 °C on HTDSC plot is due to crystallization formation while the peak starting at 560 °C is due to m-to-t transition.

was 20 ml/min. It could be noted from the top graph that during heat treatment the fibers had two major weight losses, represented by two peaks on the DTA curve. Correspondingly, the HTDSC curve showed two opposite thermal events around the same temperature ranges as the TGA graph: an endothermic process that was identified to start from room-temperature to 270 °C, and an exothermic process from 270 to 450 °C. It is believed that the first major weight loss, with mass reduction of 23%, was due to evaporation of residual moisture and ethanol content in the fibers, which would be heat-absorbing process by its nature and thus is in agreement with HTDSC result; the second major weight loss, starting at 270 °C with mass reduction of 23.5%, resulted from the decomposition and burning off of PVP polymers and other minor organic constituents introduced from the original zirconia colloid. Thus it seems reasonable to conclude that in air atmosphere the onset temperature for PVP decomposition is 270 °C.

It also came to our attention that another two exothermic events took place later on the HTDSC curve while on the TGA graph no significant weight losses were seen. With the help of NETZSCH Proteus Thermal Analysis (software ver. 5.01), the onset temperatures for these two exothermic processes were identified to be 450 and 560 °C, respectively. These two events were attributed to crystallization formation and solid-state transitions of ceramic zirconia nanofibers, which would be discussed later in Section 3.3. A weight loss of 2.5% at the end of the TGA curve is attributed to pyrolysis of residual organics entrapped inside the fibers. TGA results also show that ~51% of total weight was retained by the end of TGA test ending at 1000 °C.

3.2. HTDSC measurements of phase transitions

Fig. 3 shows two segments of HTDSC testing results of zirconia nanofibers. For all measurements, temperature ramp and air flow rate were maintained at 20 °C/min and 20 ml/min, respectively. It could be seen that the heating processes (Fig. 3 top) exhibit clear endothermic events (except for the first-run curve) while in cooling (Fig. 3 bottom) the reverse exothermic events showed up. These thermal events are strongly related to zirconia's crystal structure changes, i.e., endothermic events during heating are due to m-to-t transitions and exothermic events during cooling resulted from the reverse t-to-m transitions, which are in agreement with literature [22,23]. Some researchers [24,25] indicated that only peak temperatures (T_{pk}) on HTDSC curves may not be accurate representations of the real transition temperatures (T_{tra}); the onset (T_{on}) and offset (T_{off}) temperatures should be taken into consideration for better illustration. Herein T_{on}, T_{pk} and T_{off} were identified and determined with NETZSCH Proteus Thermal Analysis (software ver. 5.01). The results are listed in Table 1 for reference.

As Fig. 3 (top) shows, the first heating curve appeared flat around 1197 °C where endothermic events exhibited in all the rest heating processes. We repeated the tests using as-spun fibers several times and all indicated no measurable endothermic event for the first heating circle. While looking at the first cooling curve in Fig. 3 (bottom), an exothermic peak was

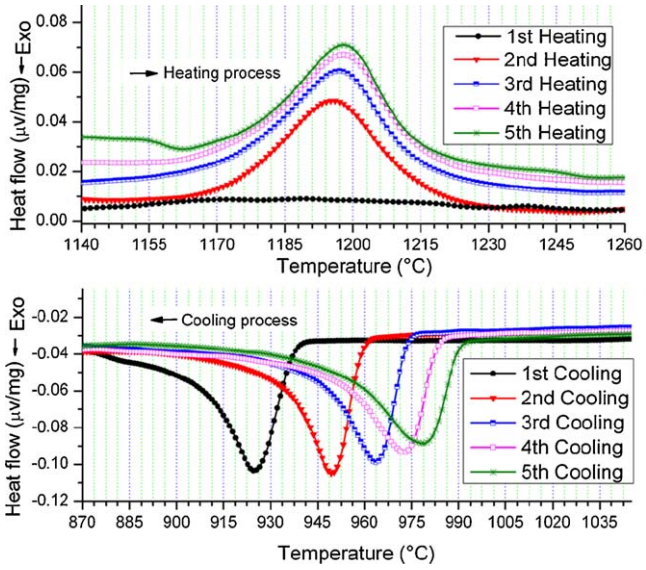

Fig. 3. Two segments of HTDSC testing results of 5 consecutive thermal circles of zirconia nanofibers. Top: heating processes; bottom: cooling processes. Endothermic events on heating, which represented m-to-t transitions, and exothermic events on cooling, which represented the reverse t-to-m transitions, could be clearly identified (except for the first heating process). The heating peak temperatures practically remained unchanged while during cooling they showed dramatic shift.

identified representing t-to-m transition, which means m-to-t transformation must have happened at heating. We believe there must have been some exothermic processes taking place at around 1197 °C that cancelled out the absorbed heat resulted from m-to-t transition, making the first heating curve look flat. One such process could be the grain growth under high temperatures, as evidenced by FESEM results that will be discussed later.

For the purpose of simplicity, T_{pk} was assumed to be T_{tra} in the following discussion. It could be noted from Table 1 that during heating, the m-to-t temperatures stayed around 1197 °C for all 4 thermal circles while in the cooling process they systemically shifted from 924.9 for the first circle to 978.6 °C for the fifth circle. It is well established that the t-to-m transitions of zirconia system are strongly particle-size dependant [23], i.e., in nanoscale smaller particles will lead to stabilization of m-phase at lower temperatures. Therefore, the temperature increase during cooling is ascribed to particle

Table 1
Comparison of onset (T_{on}), peak (T_{pk}), and offset (T_{off}) temperatures during different thermal circles.[a].

	Heating			Cooling		
	T_{on} (°C)	T_{pk} (°C)	T_{off} (°C)	T_{on} (°C)	T_{pk} (°C)	T_{off} (°C)
1st circle	–	–	–	908.2	924.9	937.4
2nd circle	1172.8	1195.5	1215.9	934.3	949.6	959.3
3rd circle	1173.1	1197.0	1216.1	945.0	963.6	973.3
4th circle	1172.8	1197.9	1216.3	951.4	972.7	983.1
5th circle	1175.1	1198.0	1213.9	953.9	978.6	989.9

[a] One thermal circle refers to heating up to 1370 from 100 °C and cooling down back to 100 °C.

growth during each thermal circle. In this respect the heating behavior would then seem somehow unreasonable because they did not show consistent shift as cooling process did. Mayo et al. [22] observed and reported the same heating phenomenon, explaining that the presence of twin interferences had made the ''apparent'' grain size equal during different heating processes, which would lead to m-to-t transitions taking place around the same temperature. We believed that is also the case here.

3.3. XRD investigation

To reveal and examine phase change and transformations of zirconia nanofibers at different calcination stages, as-spun fibers annealed to temperatures of 450, 560, 800, 900, 1000 °C in HTDSC were cooled down and XRD analyses were carried out afterwards. During annealing, the temperature ramp was 10 °C/min for heating and 20 °C/min for cooling and air flow was maintained at 20 ml/min.

The obtained XRD patterns were refined and indexed by Rietveld technique. The refined XRD spectra as well as standard JCPDS peak information for t- and m- zirconia are shown in Fig. 4. As shown in Fig. 4, no peaks were identified for fibers heated up to 450 °C, which means they still took noncyrstalline form; when temperature was raised to 560 °C, t-phase instead of m-phase exhibited clearly and explicitly, which explained the exothermic event in Fig. 2 (bottom) from 450 to 560 °C as a crystallization formation process. Similar thermodynamic process was reported on YSZ material [26]. The t- and m-phase that showed later were identified to have JCPDS no. 79-1771 and 37-1484, respectively. It seems the initial crystal phase right after crystallization formation depends strongly on sample preparation methods since initial m-phase [14], t-phase [27] and c-phase [28] were all reported although it was stated that generally t-form was the preferential phase during crystallization of amorphous zirconia [29].

When annealing temperatures were gradually lifted to 800, 900, and 1000 °C, the m-phase started to show itself steadily and its intensity rose while the t-phase faded away until finally disappeared when samples were heated to 1000 °C. While

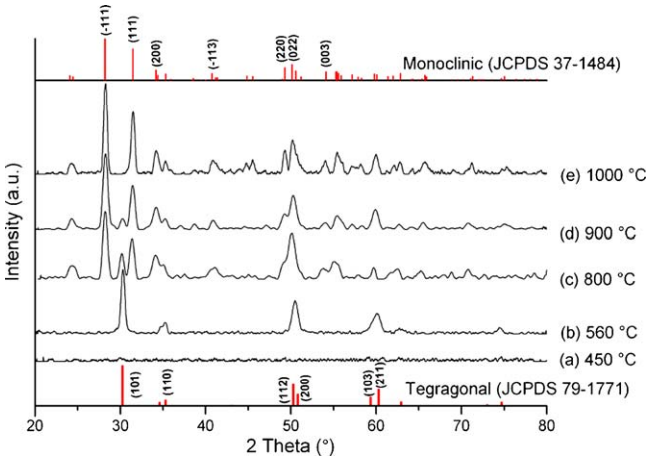

Fig. 4. XRD spectra of zirconia nanofibers annealed in HTDSC to 450 °C (a), 560 °C (b), 800 °C (c), 900 °C (d), 1000 °C (e). Standard JCPDS data for t- and m- zirconia are provided as references.

checking HTDSC plot from 560 °C up to 1000 °C in Fig. 2 (bottom), a relatively broad exothermic peak was detected. Thus it was believed this thermal event corresponds to the t-to-m phase transition. As compared to transformations of the same nature during cooling, this one happened during first heating only and had a lower onset temperature although they both released heat.

3.4. Surface morphology inspections

Zirconia nanofibers were characterized by FESEM both before and after HTDSC calcinations. During annealing, the temperature ramp was 20 °C/min and air flow rate was maintained at 20 ml/min.

Typical FESEM images of the as-spun nanofibers are displayed in Fig. 5. It is obvious that long, smooth, uniform and bead-free fibers were successfully fabricated on a large scale, with fiber diameters ~300 nm.

Fig. 6 shows zirconia fibers that were calcined to 1000 °C (left) and 1370 °C (right), respectively. From Fig. 6 (left), it could be first noted that after decomposition of PVP polymers,

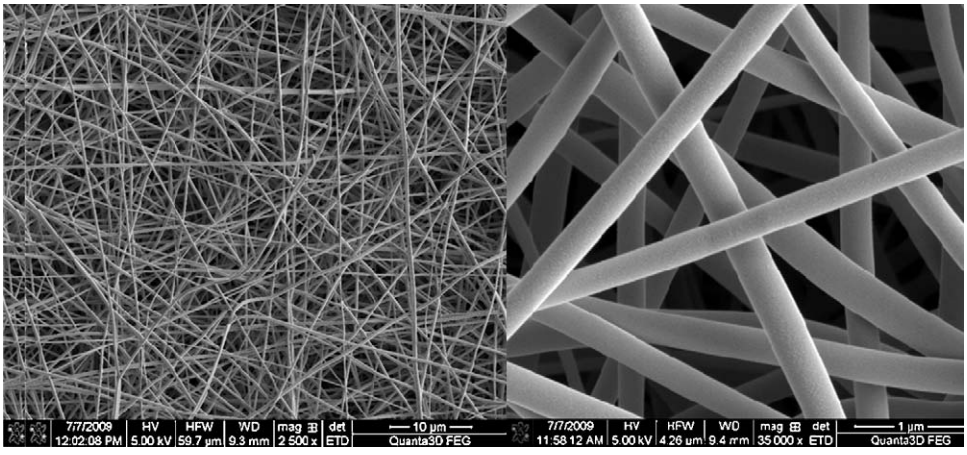

Fig. 5. FESEM images of as-spun zirconia-polymer nanofibers.

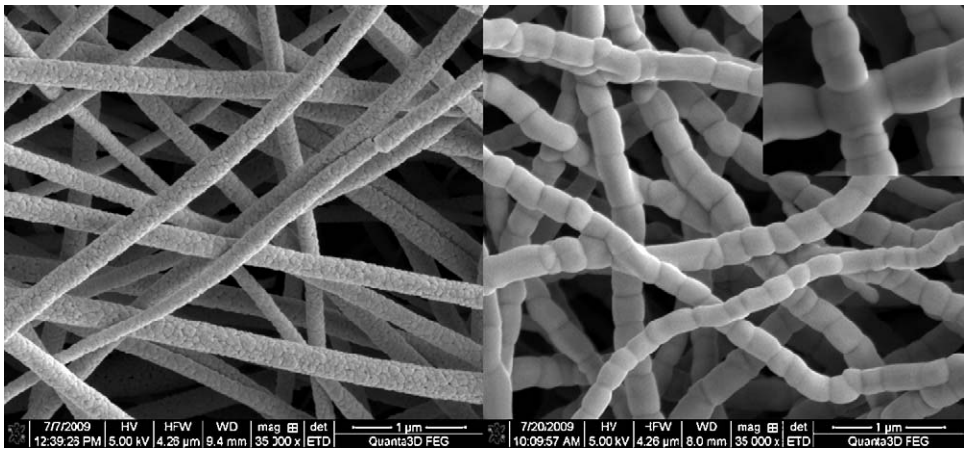

Fig. 6. FESEM images of zirconia nanofibers calcined at 1000 °C (left) and 1370 °C (right) using HTDSC; inset at right shows typical bridging of two intersecting fibers.

the fibers' original cylindrical shape and continuity were retained and no dramatic shrinkage in diameter could be detected when compared to Fig. 5 (right). Also, zirconia grains with sizes of ~50 nm were found arraying tightly against each other with micro-pores present. The grain boundaries are clearly shown as grooves, which roughened the fiber surfaces dramatically. The fibers' microstructure evolution after heat treatment was classically analyzed and theorized by Mullins [30] and was named ''thermal (grain boundary) grooving''. It is believed that grooving will occur whenever the stationary grain boundaries of a polycrystal merge to intersect the surface under high temperature. Mullins [30] also proposed two mechanisms for thermal grooving: one being evaporation–condensation and the other surface diffusion. Here, we believe surface diffusion was the dominant driving force since no appreciable fiber shrinkage was detected. In literature the same mechanism was suggested for zirconia [31,32].

When calcination temperature was raised to 1370 °C from 1000 °C (Fig. 6 (right)), further grain growth took place and the so-called ''bamboo wires'' are apparent, where the grain growth is pinned by thermal grooving in fibers when grain size is about the same as fiber diameter, leaving no pores behind. Also, as shown in the inset of Fig. 6 (right), some fibers were found bridging and joining together at the intersections where they were believed to have just barely touched each other originally. The observed mass-transport phenomena from Fig. 6 (left) to (right) were primarily attributed to volume diffusion since the deletion of pores could not result from either surface diffusion or evaporation–condensation mechanisms [31]. Because grain bridging is favorable at temperatures of 1200 °C and above for zirconia systems [31], Fig. 6 (right) also revealed that heat treatment at temperature of 1370 °C is sufficient to heal intergranular pores by sintering of neighboring grains.

Fig. 7 shows zirconia fibers that went through 5 thermal circles in HTDSC between 100 and 1370 °C. When compared to Fig. 6 (right), it could be noted that more shrinkage and necking at grain boundaries took place; the grains grew longer, which means the equivalent-particle-size have increased and thus also explained the temperature increase in the t-to-m transition in the HTDSC tests shown in Fig. 3 (bottom). It is also worthwhile to mention that in Fig. 7 bridging and joining of fibers happened extensively and they altogether formed an interconnected nano-sized zirconia network.

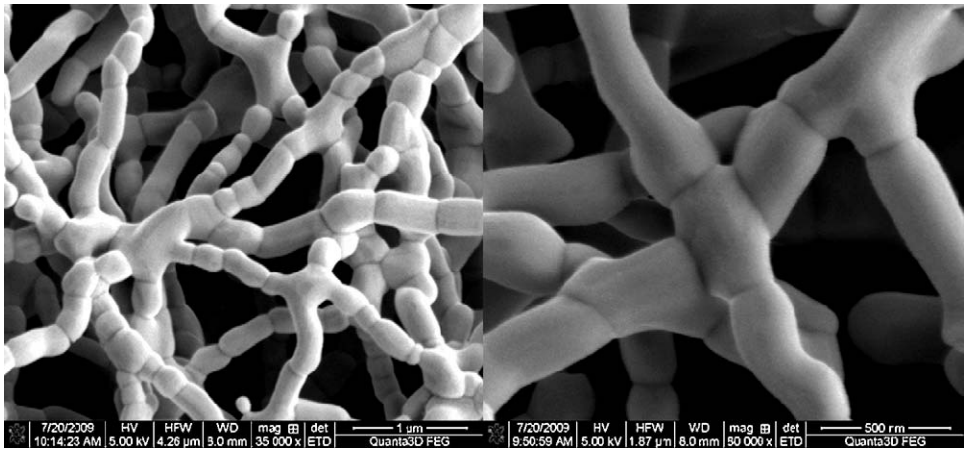

Fig. 7. FESEM images of zirconia nanofibers after 5 circles in HTDSC each heated to 1370 °C.

4. Conclusions

Zirconia nanofibers with diameters of ~300 nm were fabricated using zirconia dispersion and polymer solution on a novel electrospinning apparatus. The nanofibers were found to start crystallization in the form of t-phase at 450 °C, showing an endothermic event on corresponding HTDSC curve; another endothermic peak from 650 to ~900 °C was confirmed by XRD to be m-to-t phase transition; nanofibers showed dramatically different thermodynamic behaviors for heating and cooling processes during treatment of 5 consecutive thermal circles: m-to-t transition temperatures remained around 1197 °C on heating for all 4 circles while on cooling t-to-m temperatures increased from 924.9 °C for the first circle to 978.6 °C for the fifth. FESEM investigation revealed zirconia fibers calcined to 1000 °C showed thermal grooving, which was attributed to surface diffusion during heat treatment; fibers fired to 1370 °C formed the so-called ''bamboo wires'' while bridging and joining of fibers that went through 5 thermal circles to 1370 °C were so prevailing that they altogether formed an interconnected nano-sized zirconia network.

Acknowledgements

This work was supported by Louisiana Board of Regents under contract LEQSF (2007-10)-RD-A-08; the authors are grateful to Dr. Dongmei Cao in MMC at Louisiana State University for help and convenience she offered on FESEM usage and operations.

References

[1] Li Dan, Herricks Thurston, Xia Younan, Magnetic nanofibers of nickel ferrite prepared by electrospinning, Appl. Phys. Lett. 83 (2003) 4586.
[2] Zhang Daming, Chang Jiang, Electrospinning of three-dimensional nanofibrous tubes with controllable architectures, Nano Lett. 8 (2008) 3283.
[3] Liu Weimin, Chen Yunxia, Ye Chengfeng, Pingyu S Zhang, Preparation and characterization of doped sol-gel zirconia film, Ceram. Int. 28 (2002) 349.
[4] Guo Gong-Yi, Chen Yu-Li, Preparation an characterization of a novel zirconia precursor, Ceram. Int. 30 (2004) 469.
[5] P.K. Wright, A.G. Evans, Mechanisms governing the performance of thermal barrier coatings, Curr. Opin. Solid State Mater. Sci. 4 (1999) 25.
[6] Hansch Ralf, Mohammad Rahul Reza Chowdhury, H. Menzler Norbert, Screen printing of sol-gel-derived electrolytes for solid oxide fuel cell (SOFC) application, Ceram. Int. 35 (2009) 803.
[7] Luping Li, Peigen Zhang, Ranran Liu, S.M. Guo, Preparation of Ni-YSZ nanofiber composite as fuel cell anode material, Solid State Ionics, submitted for publication.
[8] Zhuiykov Serge, Miura Norio, Development of zirconia-based potentiometric NO*x* sensors for automotive and energy industries in the early 21st century: what are the prospects for sensors, Sens. Actuators B 121 (2007) 639.
[9] A.A. Demkov, Investigating alternative gate dielectrics: a theoretical approach, Phys. Status Solidi B 226 (2001) 57.
[10] A. Adamski, Z. Sojka, K. Dyrek, M. Che, An XRD and ESR study of V_2O_5/ZrO_2 catalysts: Influence of the phase transitions of ZrO_2 on the migration of V_4^+ ions into zirconia, Solid State Ionics 117 (1999) 113.
[11] Nath Shekhar, Sinha Nikhil, Basu Bikramjit, Microstructure, mechanical and tribological properties of microwave sintered calcia-doped zirconia for biomedical applications, Ceram. Int. 34 (2008) 1509.
[12] Margha Fatma Hassan, Abdel-Hameed Salwa Abdel-Hameed Mohamed, Ghonim Nagwa Abd El-Shafy, Ali Saadia Ahmed, Kato Shigeru, Satokawa Shigeo, Kojima Toshinori, Crystallization behavior and hardness of glass ceramics rich in nanocrystals of ZrO_2, Ceram. Int. 35 (2009) 1133.
[13] Yuli Chen, Gongyi Guo, Preparation and characterization of yttria-stabilized zirconia powders by solvent extraction process, Ceram. Int. 23 (1997) 267.
[14] G.H Latha Kumari, W.Z. Du, R. Li, S.K. Selva Vennila, D.Z. Wang Saxena, Synthesis, microstructure and optical characterization of zirconium oxide nanostructures, Ceram. Int. 35 (2009) 2401.
[15] Miao Xigeng, Sun Dan, Hoo Pui Woon, Liu Jianli, Hu Yifei, Chen Yanming, Effect of titania addition on yttria-stabilised tetragonal zirconia ceramics sintered at high temperatures, Ceram. Int. 30 (2004) 1041.
[16] Chraska Tomas, H. King Alexander, C. Berndt Christopher, On the size-dependent phase transformation in nanoparticulate zirconia, Mater. Sci. Eng. A 286 (2000) 169.
[17] W.Z. Zhu, Grain size dependence of the transformation temperature of tetragonal to monoclinic phase in $ZrO_2(Y_2O_3)$ ceramics, Ceram. Int. 22 (1996) 389.
[18] Wong Shing-Chung, Baji Avinash, Leng Siwei, Effect of fiber diameter on tensile properties of electrospun poly(ε-caprolactone), Polymer 49 (2008) 4713.
[19] Sigmund Wolfgang, Yuh Junhan, Park Hyun, Maneeratana Vasana, Pyrgiotakis Georgious, Daga Amit, Taylor Joshua, C. Nino Juan, Processing and structure relationships in electrospinning of ceramic fiber systems, J. Am. Ceram. Soc. 89 (2) (2006) 395.
[20] Laforgue Alexis, Robitaille Lucie, Mokrini Asmae, Ajji Abdllah, Fabrication and characterization of ionic conducting nanofibers, Macromol. Mater. Eng. 292 (2007) 1229.
[21] Yaqi Shunsuke, Nakagawa Tomoki, Matsubara Eiichiro, Matsubara Seijiro, Ogawa Satoshi, Tani Hiroshi, Formation of tin nanoparticles embedded in poly(L-lactic acid) fiber by electrospinning, Electrochem. Solid-State Lett. 11 (2008) E25.
[22] M.J. Mayo, A. Suresh, W.D. Porter, Thermodynamics for nanosystems: grain and particle-size dependent phase diagrams, Rev. Adv. Mater. Sci. 5 (2003) 100.
[23] Suresh Arun, J. Mayo Merrilea, Crystallite and grain-size-dependent phase transformations in yttria-doped zirconia, J. Am. Ceram. Soc. 86 (2) (2003) 360.
[24] Moriya Yosuke, Navrotsky Alexandra, High-temperature calorimetry of zirconia: Heat capacity and thermodynamics of the monoclinic-tetragonal phase transition, J. Chem. Thermodyn. 38 (2006) 211.
[25] M. Sorai (Ed.), Comprehensive Handbook of Calorimetry and Thermal Analysis, Wiley, New York, 2004.
[26] K. Prabhakaran, M.O. Beigh, J. Lakra, N.M. Gokhale, S.C. Sharma, Characteristics of 8 mol% yttria stabilized zirconia powder prepared by spray drying process, J. Mater. Process. Technol. 189 (2007) 178.
[27] Lin Cuikun, Zhang Cuimiao, Lin Jun, Phase transformation and photoluminescence properties of nanocrystalline ZrO_2 powders prepared via the Pechini-type sol-gel process, J. Phys. Chem. C 111 (2007) 3300.
[28] C. Ray Jagadish, K. Ranjan, P. Pramanik Pati, Chemical synthesis and structural characterization of nanocrystalline powders of pure zirconia and yttria stabilized zirconia (YSZ), J. Eur. Ceram. Soc. 20 (2000) 1289.
[29] G.-Y. Guo, Y.-L. Chen, Unusual structural phase transition in nanocrystalline zirconia, Appl. Phys. A 84 (2006) 431.
[30] W.W. Mullins, Theory of thermal grooving, J. Appl. Phys. 28 (3) (1957) 333.
[31] A. Erk Kendra, Deschaseaux Christophe, W. Trice Rodney, Grain-boundary grooving of plasma-sprayed yttria-stabilized zirconia thermal barrier coatings, J. Am. Ceram. Soc. 89 (5) (2006) 1673.
[32] M.J. Mayo Akash, Zr surface diffusion in tetragonal yttria stabilized zirconia, J. Mater. Sci. 35 (2000) 437.